Effects of interaction between ultramafic tectonite and mafic magma on Nd-Pb-Sr isotopic systems in the Neoproterozoic Chaya Massif, Baikal-Muya ophiolite belt

Article *in* Earth and Planetary Science Letters · April 1997

CITATIONS
29

READS
38

3 authors, including:

Yuri Amelin
Australian National University
245 PUBLICATIONS **8,247** CITATIONS

SEE PROFILE

Leonid A. Neymark
United States Geological Survey
155 PUBLICATIONS **1,707** CITATIONS

SEE PROFILE

ELSEVIER

Earth and Planetary Science Letters 148 (1997) 299–316

EPSL

Effects of interaction between ultramafic tectonite and mafic magma on Nd–Pb–Sr isotopic systems in the Neoproterozoic Chaya Massif, Baikal–Muya ophiolite belt

Yuri V. Amelin [a,b,*], Eugeni Yu. Ritsk [a], Leonid A. Neymark [a,c]

[a] *Institute of Precambrian Geology and Geochronology, 2 Makarova emb., St. Petersburg, 199034, Russia*
[b] *Geochronology Laboratory, Royal Ontario Museum, 100 Queen's Park, Toronto, Ont. M5S 2C6, Canada*
[c] *U.S. Geological Survey, Denver Federal Center, Box 25046, M.S. 963, Denver, CO 80225, USA*

Received 5 June 1996; revised 18 February 1997; accepted 25 February 1997

Abstract

Sm–Nd, Rb–Sr and U–Pb isotopic systems have been studied in minerals and whole rocks of harzburgites and mafic cumulates from the Chaya Massif, Baikal–Muya ophiolite belt, eastern Siberia, in order to determine the relationship between mantle ultramafic and crustal mafic sections. Geological relations in the Chaya Massif indicate that the mafic magmas were emplaced into, and interacted with older solid peridotite. Hand picked, acid-leached, primary rock-forming and accessory minerals (olivine, orthopyroxene, clinopyroxene and plagioclase) from the two harzburgite samples show coherent behavior and yield $^{147}Sm/^{144}Nd$–$^{143}Nd/^{144}Nd$ and $^{238}U/^{204}Pb$–$^{206}Pb/^{204}Pb$ mineral isochrons, corresponding to ages of 640 ± 58 Ma (95% confidence level) and 620 ± 71 Ma, respectively. These values are indistinguishable from the crystallization age of the Chaya mafic units of 627 ± 25 Ma (a weighted average of internal isochron Sm–Nd ages of four mafic cumulates). The Rb–Sr and Sm–Nd isotopic systems in the harzburgite whole-rock samples were disturbed by hydrothermal alteration. These alteration-related isotopic shifts mimic the trend of variations in primary isotopic compositions in the mafic sequence, thus emphasizing that isotopic data for ultramafic rocks should be interpreted with great caution.

On the basis of initial Sr and Nd values, ultramafic and mafic rocks of the Chaya Massif can be divided into two groups: (1) harzburgites and the lower mafic unit gabbronorites with $\varepsilon_{Nd} = +6.6$ to $+7.1$ and $\varepsilon_{Sr} = -11$ to -16; and (2) websterite of the lower unit and gabbronorites of the upper mafic unit: $\varepsilon_{Nd} = +4.6$ to $+6.1$ and $\varepsilon_{Sr} = -8$ to -9. Initial Pb isotopic ratios are identical in all rocks studied, with mean values of $^{206}Pb/^{204}Pb = 16.994 \pm 0.023$ and $^{207}Pb/^{204}Pb = 15.363 \pm 0.015$. The similarity of ages and initial isotopic ratios within the first group indicates that the isotopic systems in the pre-existing depleted peridotite were reset by extensive interaction with basaltic magma during formation of the mafic crustal sequence. The isotopic data agree with a hypothesized formation of the Chaya Massif in a suprasubduction-zone environment.

Keywords: Chaya Massif; isotopes; tectonite; mafic magmas; geochemistry

* Corresponding author. Present address: Geochronology Laboratory, Royal Ontario Museum, 100 Queen's Park, Toronto, ON M5S 2C6, Canada. Tel.: +1 416 586 5811. Fax: +1 416 586 5814. E-mail: yuria@rom.on.ca

PII S0012-821X(97)00046-0

1. Introduction

The relationship between mantle ultramafic tectonites (harzburgite, dunite) and crustal mafic magmatites in ophiolite complexes is a key question to understanding the processes of creation of oceanic crust. The importance of establishing the relative chronology of ultramafic tectonites and mafic magmatites is now recognized [1] but the isotopic studies that address this problem are scarce and mostly rely on whole-rock isochron relationships [2,3] that assume uniformity of initial isotopic ratios. The only exception, to our knowledge, is the study of the Trinity ophiolite by Jacobsen et al. [4] that demonstrated by mineral isochron Sm–Nd dating that a plagioclase lherzolite and mafic dikes in this complex are not coeval and have distinct initial Nd isotopic ratios.

The aim of this study is to establish temporal and genetic relationships between peridotites and mafic rocks in a Precambrian ophiolite complex. We report the isotopic data, as well as major and rare earth element concentrations, for harzburgites and mafic cumulates from the Chaya Massif in the late Proterozoic Baikal–Muya ophiolite belt, eastern Siberia. To determine ages and initial isotopic ratios, we have studied a number of rock-forming and accessory minerals, along with whole-rock samples, from

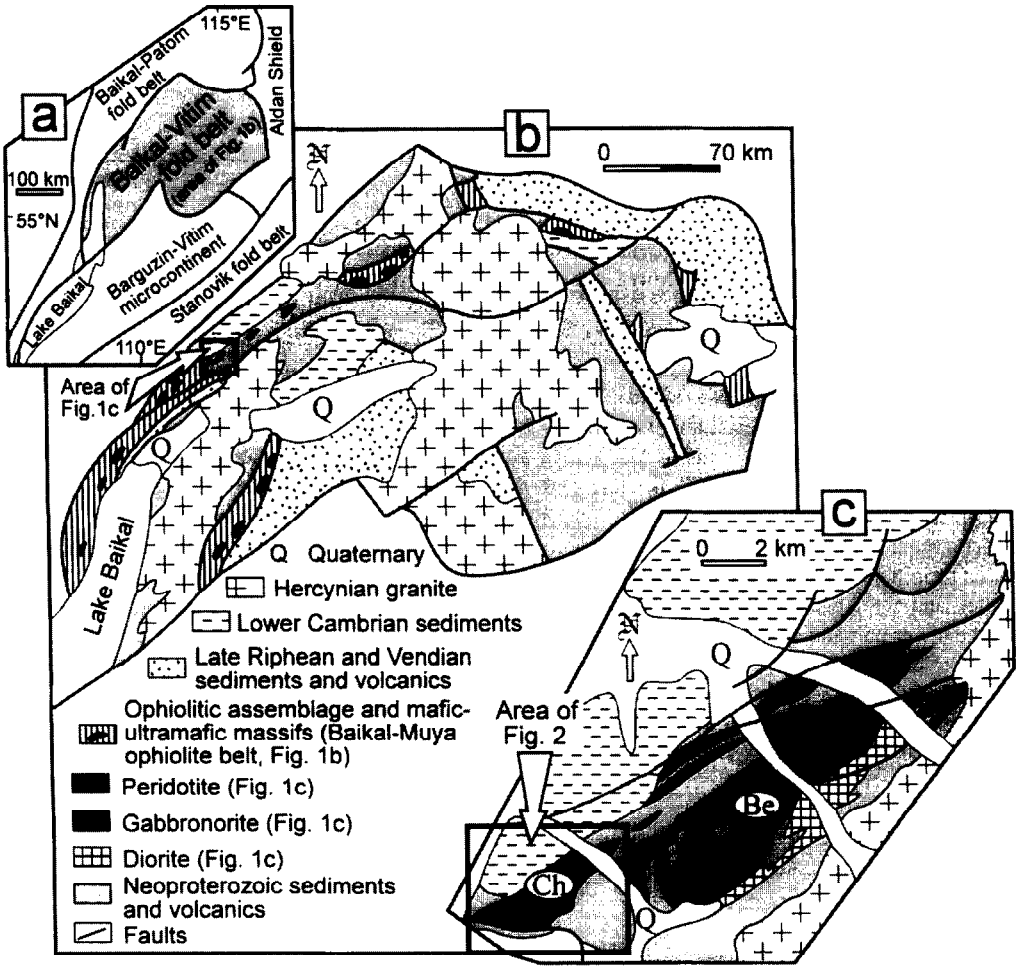

Fig. 1. (a) Map of Southeastern Siberia, showing: (b) the position of the Baikal–Muya ophiolite belt, and (c) tectonic setting of the Chaya Massif. *Ch* = Chaya Massif; *Be* = Bezymianny Massif.

harzburgites and mafic cumulates using Sm–Nd, U–Pb and Rb–Sr techniques.

2. Geological setting

The Baikal–Muya ophiolite belt (Fig. 1a,b) is a wide belt of ultramafic and mafic plutons and mafic metavolcanics that extends from the northern coast of Lake Baikal to the northeast for more than 500 km. First recognized as an ophiolite belt by Klitin and Pavlova [5], the Baikal–Muya belt in now interpreted as having been formed during the evolution of the Neoproterozoic Paleo-Asian Ocean [6]. Geological features of the Baikal–Muya belt and the tectonic settings of its segments are summarized in [7–11].

The Chaya zoned ultramafic–mafic Massif (Fig. 1c and 2) is localized within the amphibolite-grade Neoproterozoic volcano-sedimentary sequence composed of metasandstones and schists, interlayered with basic and felsic volcanics, and is overlain by lower Cambrian molasse. The Chaya Massif is structurally associated with the Bezymianny gabbro–diorite Massif (Fig. 1c). Most of the exposed contacts between mafic rocks of the Chaya and Bezymianny massifs and the basement are magmatic, with hornfels in the host rocks and a chilled zone in the margin of the intrusive. The southwestern basal contact of the Chaya Massif is tectonized along a shear zone and contains serpentinite melange. Hydrothermal alteration in the Chaya and Bezymianny massifs, as well as late folding and retrograde metamorphism

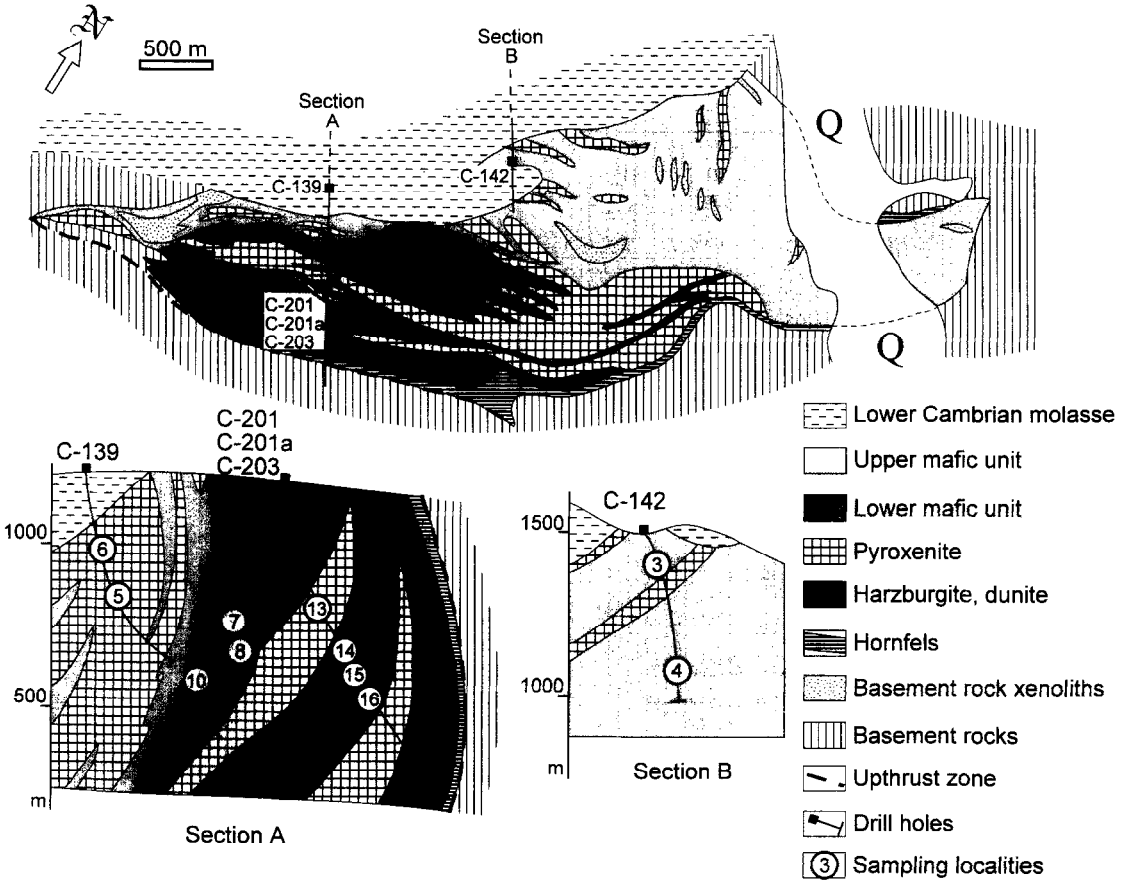

Fig. 2. Geological map of the Chaya massif, based on data from A.G. Stepin and the present authors.

in the basement rocks, may be related to the accretion and obduction on the continental margin (Ritsk et al., in prep.).

The Chaya Massif includes three main lithological units (Fig. 2): lower and upper mafic cumulative units and the middle harzburgite core, separated by pyroxenite zones. Geological relationships and the petrography of the Chaya Massif are described in detail by Lesnov [12]. The lower and upper mafic units consist of massive and trachytoid gabbronorite and norite, composed of primary orthopyroxene, clinopyroxene and plagioclase. The middle ultramafic unit is composed of variably serpentinized harzburgite and subordinate dunite, mostly with granoblastic texture; translation twinning is broadly developed. Deformation structures are clearly revealed in more extensively serpentinized harzburgite varieties. Orthopyroxenite and minor websterite, norite and plagioclase-bearing peridotite compose the pyroxenite zone surrounding the harzburgite core, and occur in lesser amounts within the gabbronorite units. Gabbronorite and pyroxenite cross-cut tectonite fabrics in the harzburgite and dunite, with the formation of breccias and harzburgite xenoliths. The localization of gabbronorite and pyroxenite veins within the harzburgite is controlled by fracturing. Gabbronorite veins emplaced into harzburgite are surrounded by 5–10 cm pyroxenite reaction zones. These relationships indicate that the parental magmas of the mafic units were emplaced into, and interacted with, older solid, relatively cold peridotite.

The geodynamic environment of the Chaya Massif formation is not precisely established. According to Dobretsov [13], the mafic plutons in the 'outer zone' of the Baikal–Muya belt, including the Chaya Massif, may have been formed at a rifted passive continental margin by a process similar to the initial stage of the Red Sea opening. Alternatively, these mafic plutons may be a part of an island arc assemblage together with spatially associated calc-alkaline

Table 1
Major element and REE data

Sample:	Ch-3	Ch-4	Ch-5	Ch-6	Ch-7	Ch-8	Ch-10	Ch-13	Ch-14	Ch-15	Ch-16
Rock:	GN	GN	Webs	OP	Harz	Harz	Harz	Webs	GN	GN	GN
SiO_2 (wt%)	52.26	50.31	51.82	53.06	37.98	37.49	39.08	52.36	50.28	51.81	50.35
TiO_2	0.24	0.05	0.08	0.06	b.d.l.	b.d.l.	b.d.l.	0.08	0.08	0.15	0.31
Al_2O_3	10.89	15.06	4.24	3.78	2.10	1.43	2.25	6.05	15.29	11.42	7.55
Fe_2O_3	2.49	1.65	1.80	2.59	4.37	3.13	3.95	2.02	3.95	1.60	2.68
FeO	5.72	4.52	8.05	7.96	9.99	9.87	9.81	6.90	3.65	4.71	5.40
MnO	0.10	0.02	0.10	0.10	0.11	0.12	0.13	0.11	0.04	0.09	0.11
MgO	17.64	16.05	27.33	29.50	42.95	45.64	43.91	22.91	14.46	19.11	19.18
CaO	9.11	9.91	4.46	1.98	0.57	b.d.l.	0.22	9.05	10.22	9.07	12.65
Na_2O	1.28	1.41	0.26	0.06	0.10	0.05	0.15	0.49	1.57	1.07	0.92
K_2O	0.05	0.01	b.d.l.	0.05	b.d.l.	b.d.l.	b.d.l.	0.01	0.06	0.10	0.02
P_2O_5	b.d.l.	0.01	b.d.l.	b.d.l.	b.d.l.	b.d.l.	b.d.l.	b.d.l.	b.d.l.	b.d.l.	0.01
LOI	2.68	0.74	0.77	0.15	2.94	2.06	2.20	0.76	1.23	1.03	2.01
Mg #	0.796	0.826	0.833	0.835	0.845	0.864	0.853	0.822	0.780	0.845	0.812
La (ppm)		0.794	0.222	0.207		0.070	0.084		1.24		1.28
Ce		2.44	0.828	0.645		0.174	0.246		3.05		4.85
Nd		2.48	0.973	0.610		0.124	0.188		2.30		5.26
Sm		0.830	0.372	0.221		0.035	0.055		0.674		1.77
Eu		0.313	0.116	0.707		0.012	0.018		0.336		0.587
Gd		1.05	0.507	0.313		0.042	0.065		0.805		2.20
Dy		1.20	0.659	0.449		0.049	0.077		0.870		2.37
Er		0.735	0.461	0.350		0.036	0.057		0.518		1.35
Yb		0.690	0.515	0.423		0.049	0.073		0.478		1.16

Rock name abbreviations: GN = gabbronorite; Webs = websterite; OP = orthopyroxenite; Harz = harzburgite.
Major elements recalculated volatile-free, volatiles are determined as loss on ignition (LOI).
b.d.l. = below detection limits (about 0.01% for TiO_2, K_2O and P_2O_5).
Mg# = molar MgO/(MgO + FeO).

volcanics and plutons [6,9]. In our opinion, the geological features of the Chaya Massif: the existence of solid harzburgite prior to emplacement of the mafic magmas; intrusive relationships of the mafic section with the enclosing rocks; and the formation of the enclosing volcano-sedimentary sequence in the proximity of a continent (Ritsk et al., in prep.) are consistent with the interpretation of the Chaya Massif as a deep (intrusive) part of an island arc, rather than as part of a normal oceanic crust or a post-obduction intrusion. If this is the case the harzburgites represent a remnant of pre-existing oceanic lithosphere.

Numerous K–Ar 'age determinations' for Chaya

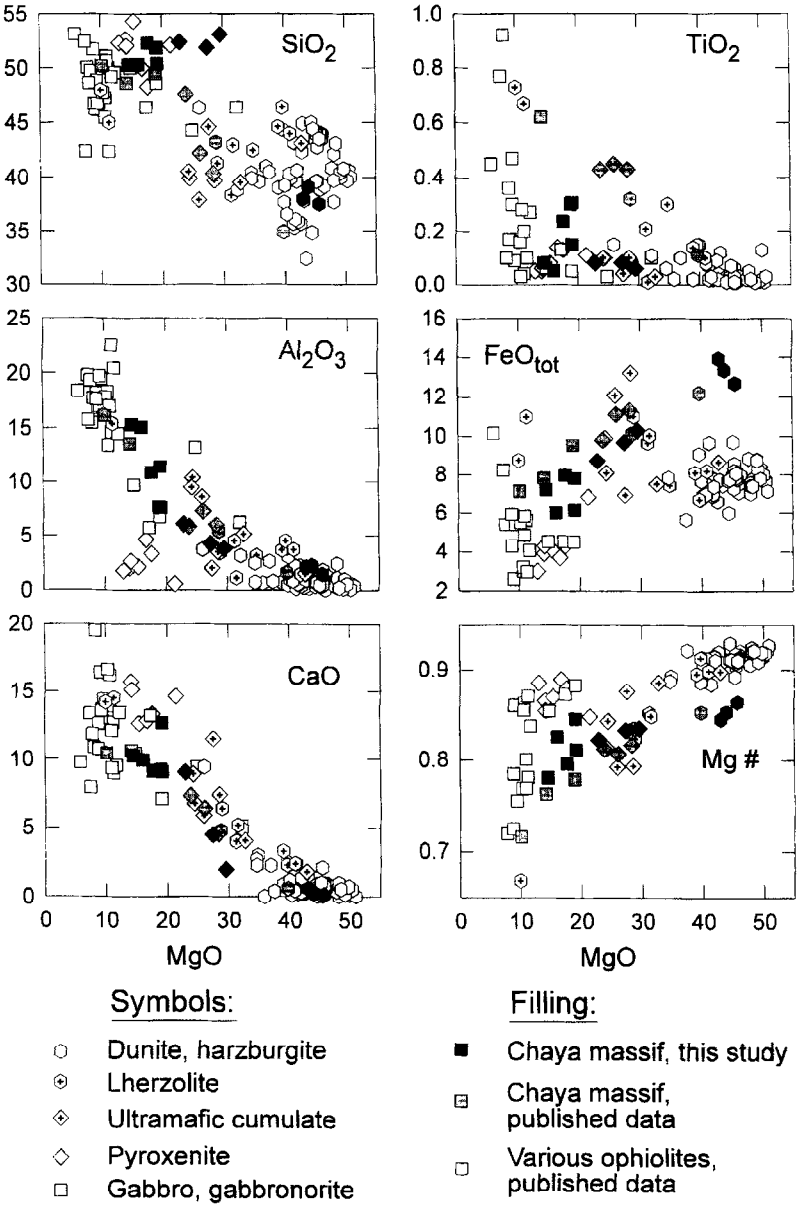

Fig. 3. Major element compositions of the samples studied from the Chaya Massif and various ophiolites. Published data for the Chaya massif (gray symbols) are from [12]; published data for other ophiolites (open symbols) are from [9,10,16,30,33,50].

mafic and ultramafic rocks were performed during the 1960s using mostly whole rocks and a few biotite separates. These data yielded a range of apparent ages from 300 to 550 Ma [12]. A Rb–Sr whole-rock–phlogopite age of ca. 737 Ma was determined by A.A. Tsygankov (personal commun.).

3. Samples

The studied samples from the Chaya Massif represent its principal lithological units (Fig. 2). The samples from the upper gabbronorite unit are melanocratic (Ch-3) and leucocratic (Ch-4) gabbronorites, composed of primary plagioclase (20–75%), orthopyroxene (15–60%) and clinopyroxene (10–20%), and secondary actinolite (< 8%) and carbonate + adularia (< 4%). The websterite Ch-5 and orthopyroxenite Ch-6 from the upper pyroxenite unit are composed of 80–90% orthopyroxene, 7–15% clinopyroxene and 7–12% secondary actinolite + talc. Harzburgites Ch-7, Ch-8 and Ch-10 are composed of 84–95% olivine (Fo88–86) + orthopyroxene and 5–15% secondary serpentine, and contain accessory clinopyroxene, plagioclase, chromian spinel, magnetite, and sulfide. The websterite Ch-13 from the lower pyroxenite unit is composed of 70% orthopyroxene, 25% clinopyroxene, 1% plagioclase, and 4% actinolite. Gabbronorites Ch-14, Ch-15 and Ch-16 from the lower gabbronorite unit are composed of plagioclase (15–35%), orthopyroxene (12–48%) and clinopyroxene (30–58%), and < 10% of secondary actinolite, talc, chlorite, carbonate and adularia.

4. Results

Isotopic data and REE concentrations were obtained using the analytical techniques described in Appendix A and in footnotes to Tables 1–3. Major element concentrations were determined by XRF.

4.1. Major element and REE concentrations

Major element and REE data are presented in Table 1. Fig. 3 shows the variations in major element concentrations versus MgO. Compared to mantle

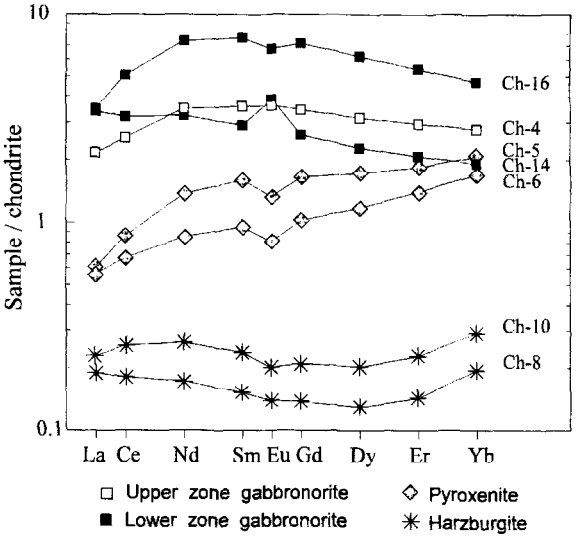

Fig. 4. Chondrite-normalized REE patterns for the Chaya ultramafic and mafic rocks. Chondrite normalization after Taylor and McLennan [51].

peridotites from the other ophiolite complexes, the Chaya harzburgites have relatively low SiO_2 and CaO, and high FeO at the same MgO. High SiO_2 (52–53 wt%) and low CaO in the Chaya pyroxenites, compared to those in typical ophiolite ultramafic cumulates, are consistent with the unusually high abundance of orthopyroxene.

Chondrite-normalized REE patterns for the Chaya whole-rock samples are shown in Fig. 4. The chondrite-normalized REE concentrations are between 0.6 and 2.5 in the pyroxenites and between 1.5 and 8 in gabbronorites. The pattern shapes closely follow mineral/basalt partition coefficients [14] and indicate the control over the REE distribution by predominant cumulus mineral species: orthopyroxene in Ch-5 and Ch-6, plagioclase in Ch-14 and clinopyroxene ± plagioclase in Ch-16 and Ch-4. The concentration range and pattern shapes of REE in the mafic–ultramafic cumulates are consistent with their crystallization from a single magma or magmas with similar N-MORB-like REE distribution.

The harzburgites have REE concentrations of about 0.2–0.3 times chondritic and are slightly enriched in both light and heavy REE with respect to middle REE (Eu, Gd and Dy). The concentrations of heavy REE (Tb and Yb) of 36–73 ppb approach those in the most depleted mantle peridotites [3,16–

Table 2
Sm–Nd and Rb–Sr data and model parameters

Sample and lithology	Fraction	Fraction weight (mg)	Lab.	Sm (ppm)	Nd (ppm)	$^{147}Sm/^{144}Nd$	$^{143}Nd/^{144}Nd$	$\varepsilon_{Nd}(627)$	Rb (ppm)	Sr (ppm)	$^{87}Rb/^{86}Sr$	$^{87}Sr/^{86}Sr$	$\varepsilon_{Sr}(627)$
Ch-3 Gabbronorite	WR	> 100	IPGG	0.578	1.907	0.1829 ± 4	0.512893 ± 21	6.1 ± 0.4	1.310	552	0.0069	0.70325 ± 4	−8.1 ± 0.7
Ch-4 Gabbronorite	WR	> 100	IPGG	0.896	2.712	0.1998 ± 5	0.512913 ± 21	5.2 ± 0.4	1.100	207	0.0153	0.70331 ± 4	−8.3 ± 0.6
Ch-4 Gabbronorite	Pl	> 100	IPGG	0.200	1.459	0.0828 ± 2	0.512427 ± 23	5.1 ± 0.5					
Ch-4 Gabbronorite	Opx	> 100	IPGG	0.126	0.329	0.2299 ± 10	0.513018 ± 22	4.8 ± 0.4					
Ch-4 Gabbronorite	Cpx	> 100	IPGG	1.869	5.114	0.2204 ± 5	0.512998 ± 22	5.2 ± 0.4					
Ch-5 Websterite	WR	> 100	IPGG	0.299	0.792	0.2275 ± 7	0.512999 ± 23	4.6 ± 0.5	0.187	9.82	0.0550	0.70383 ± 4	−6.0 ± 0.6
Ch-6 Orthopyroxenite	WR	> 100	IPGG	0.178	0.493	0.2176 ± 5	0.512900 ± 22	3.5 ± 0.4	0.081	3.47	0.0678	0.70403 ± 4	−4.8 ± 0.6
Ch-7 Harzburgite	WR	~ 400	IPGG	0.065	0.274	0.1433 ± 4	0.512578 ± 21	3.2 ± 0.4	0.596	12.05	0.1431	0.70493 ± 4	−1.6 ± 0.6
Ch-7 Harzburgite	Pl-1	2.99	ROM	0.137	0.960	0.0860 ± 12	0.512497 ± 23	6.2 ± 0.5	0.578	1075	0.00155	0.70304 ± 4	−10.5 ± 0.7
Ch-7 Harzburgite	Pl-2	2.59	ROM	0.116	0.901	0.0777 ± 14	0.512510 ± 22	7.1 ± 0.5	1.522	973	0.0045	0.70294 ± 4	−12.2 ± 0.7
Ch-7 Harzburgite	Cpx	3.19	ROM	3.375	11.30	0.1806 ± 2	0.512940 ± 16	7.2 ± 0.3	0.099	49.0	0.0058	0.70280 ± 4	−14.3 ± 0.7
Ch-7 Harzburgite	Opx	4.70	ROM	0.539	1.636	0.1989 ± 6	0.512964 ± 17	6.2 ± 0.3	0.107	24.4	0.0127	0.70313 ± 4	−10.5 ± 0.6
Ch-7 Harzburgite	Ol	0.98	ROM	0.0140	0.0683	0.118 ± 26	0.51271 ± 20	7.8 ± 4.4	0.017	10.5	0.0047	0.70288 ± 4	−13.1 ± 0.7
Ch-8 Harzburgite	WR	~ 400	IPGG	0.0390	0.125	0.1860 ± 8	0.512727 ± 25	2.6 ± 0.5	0.115	5.39	0.0617	0.70403 ± 4	−4.0 ± 0.6
Ch-10 Harzburgite	WR	~ 400	IPGG	0.0521	0.172	0.1817 ± 6	0.512859 ± 25	5.6 ± 0.5	0.231	2.56	0.2621	0.70585 ± 4	−3.7 ± 0.9
Ch-10 Harzburgite	Cpx	8.73	ROM	2.558	7.53	0.2053 ± 3	0.513050 ± 16	7.4 ± 0.3	0.114	46.3	0.0071	0.70270 ± 4	−15.9 ± 0.7
Ch-10 Harzburgite	Opx-1	9.26	ROM	0.154	0.389	0.2387 ± 13	0.513164 ± 17	6.9 ± 0.4	0.126	5.59	0.0653	0.70324 ± 4	−15.7 ± 0.6
Ch-10 Harzburgite	Opx-2	9.68	ROM	0.408	1.170	0.2107 ± 5	0.513040 ± 20	6.8 ± 0.4	0.229	8.05	0.0824	0.70359 ± 4	−12.9 ± 0.6
Ch-10 Harzburgite	Ol	6.17	ROM	0.0015	0.0097	0.091 ± 26	0.51256 ± 18	7.1 ± 4.1	0.0064	0.075	0.248		
Ch-13 Websterite	WR	> 100	IPGG	0.189	0.587	0.1947 ± 6	0.512838 ± 24	4.1 ± 0.5	0.371	61.3	0.0175	0.70337 ± 4	−7.8 ± 0.6
Ch-13 Websterite	Pl	5.78	ROM	0.122	1.091	0.0675 ± 5	0.512344 ± 17	4.7 ± 0.4	0.515	1377	0.00108	0.70312 ± 4	−9.2 ± 0.7
Ch-13 Websterite	Cpx	6.50	ROM	2.432	7.70	0.1909 ± 2	0.512853 ± 15	4.7 ± 0.3	0.044	52.5	0.00243	0.70324 ± 5	−7.7 ± 0.7
Ch-13 Websterite	Opx	10.33	ROM	0.0958	0.233	0.2484 ± 20	0.513095 ± 20	4.8 ± 0.4	0.044	3.42	0.0369	0.70342 ± 4	−9.5 ± 0.7
Ch-14 Gabbronorite	WR	> 100	IPGG	0.681	2.443	0.1681 ± 4	0.512866 ± 23	6.8 ± 0.5	0.949	515	0.0053	0.70295 ± 4	−12.2 ± 0.7
Ch-14 Gabbronorite	Pl	> 100	IPGG	0.208	1.620	0.0775 ± 2	0.512470 ± 28	6.4 ± 0.6					
Ch-14 Gabbronorite	Opx	> 100	IPGG	0.096	0.283	0.2054 ± 10	0.513029 ± 22	7.0 ± 0.4					
Ch-14 Gabbronorite	Cpx	> 100	IPGG	1.888	5.502	0.2069 ± 5	0.512997 ± 21	6.2 ± 0.4					
Ch-15 Gabbronorite	WR	> 100	IPGG						.472	402	0.0034	0.70299 ± 4	−11.3 ± 0.7
Ch-16 Gabbronorite	WR	> 100	IPGG	2.038	6.135	0.2004 ± 5	0.513008 ± 21	7.0 ± 0.4	0.454	113	0.0117	0.70307 ± 4	−11.3 ± 0.6
Ch-16 Gabbronorite	Pl	> 100	IPGG	0.132	1.097	0.0728 ± 2	0.512449 ± 22	6.3 ± 0.5					
Ch-16 Gabbronorite	Opx	> 100	IPGG	0.168	0.459	0.2202 ± 8	0.513092 ± 22	7.0 ± 0.4					
Ch-16 Gabbronorite	Cpx	> 100	IPGG	2.017	5.864	0.2075 ± 5	0.513008 ± 22	6.4 ± 0.4					

Errors in $^{143}Nd/^{144}Nd$ and $^{87}Sr/^{86}Sr$ are 2σ, propagated to include individual within-run errors and reproducibilitity of standard analyses. $^{147}Sm/^{144}Nd$ and $^{87}Rb/^{86}Sr$ ratios and Sm, Nd, Rb and Sr concentrations are corrected for average Sm and Nd blanks. Errors in $^{147}Sm/^{144}Nd$ are 2σ, propagated to include reproducibilitity of BCR-1 standard analyses and uncertainty in blank correction. Errors in ε_{Nd} (2σ) are propagated to include uncertainties in $^{143}Nd/^{144}Nd$, $^{147}Sm/^{144}Nd$ and age. Errors in ε_{Sr} (2σ) are propagated to include uncertainties in $^{87}Sr/^{86}Sr$, $^{87}Rb/^{86}Sr$ and age.

The age of 627 ± 25 Ma is assumed for initial ratio calculations.

Pl-1 in Ch-7 is a fraction of pale brown or reddish, cloudy plagioclase fragments; Pl-2 is a fraction of colorless, clear to slightly cloudy fragments.

Opx-1 in Ch-10 is a fraction of the best grains; Opx-2 is the bulk Opx fraction.

18] and indicate strong depletion of the Chaya harzburgites. The U-shaped REE patterns, observed in the Chaya harzburgites, are common in mantle peridotites [15]. Such patterns cannot be produced by equilibrium partial melting of a source with chondritic or LREE-depleted REE distribution [16], and may be a result of peridotite contamination by a melt or fluid-bearing crustal REE signature [18]. In the latter case the Nd isotopic ratios are also likely to be shifted towards crustal values [18].

4.2. Sm–Nd systematics

The whole-rock and mineral Sm–Nd data for four mafic samples from the Chaya Massif are presented in Table 2. The internal Sm–Nd isochrons for these samples (Fig. 5) yield ages between 624 and 656 m.y., identical within error limits. Their weighted average of 627 ± 25 Ma (95% confidence level) we consider to be the best estimate for the crystallization age of the Chaya mafic units. The isochron ages and initial $\varepsilon_{Nd}(T)$ values are less precise for the lower mafic unit samples Ch-13, Ch-14 and Ch-16, showing excessive scatter of analyses in the evolution diagrams. The more precise mean $\varepsilon_{Nd}(627)$ values (Fig. 5), calculated as weighted averages of $\varepsilon_{Nd}(627)$ values for individual mineral and whole-rock analyses of each sample, fall into two distinct groups of approximately +4.9 and +6.7.

The Sm–Nd data for harzburgites Ch-7 and Ch-10

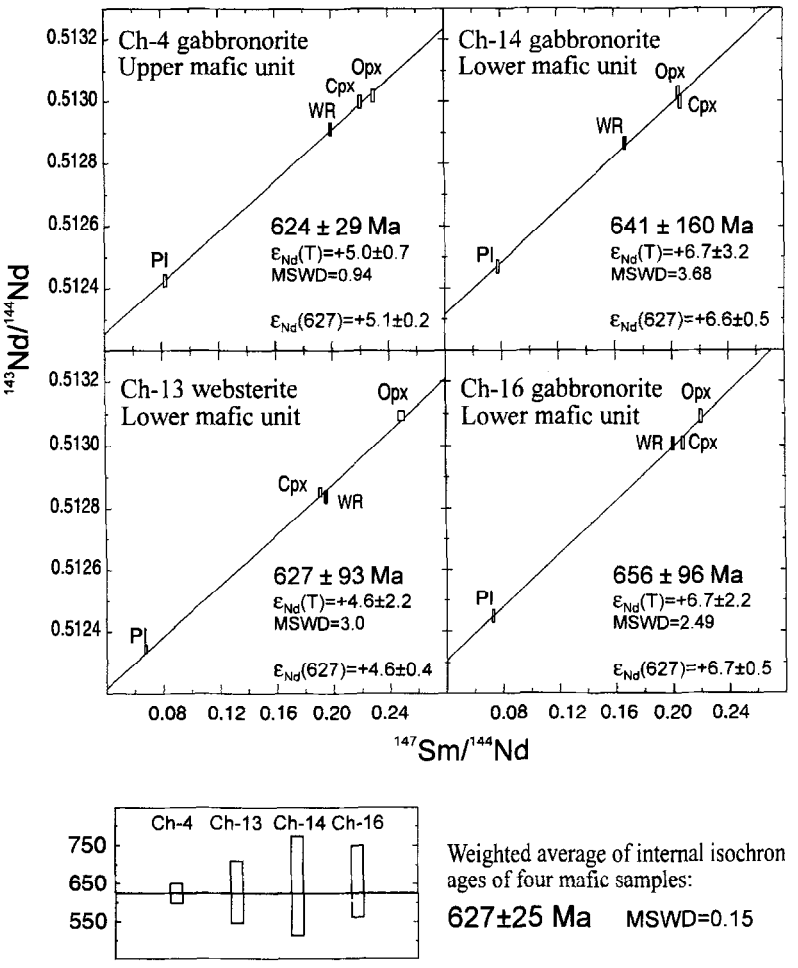

Fig. 5. Sm–Nd mineral isochrons for mafic units of the Chaya Massif. The $\varepsilon_{Nd}(T)$ values are obtained from internal isochron regressions. The $\varepsilon_{Nd}(627)$ values shown in the figure are weighted averages of $\varepsilon_{Nd}(627)$ of individual mineral and whole-rock analyses of each sample.

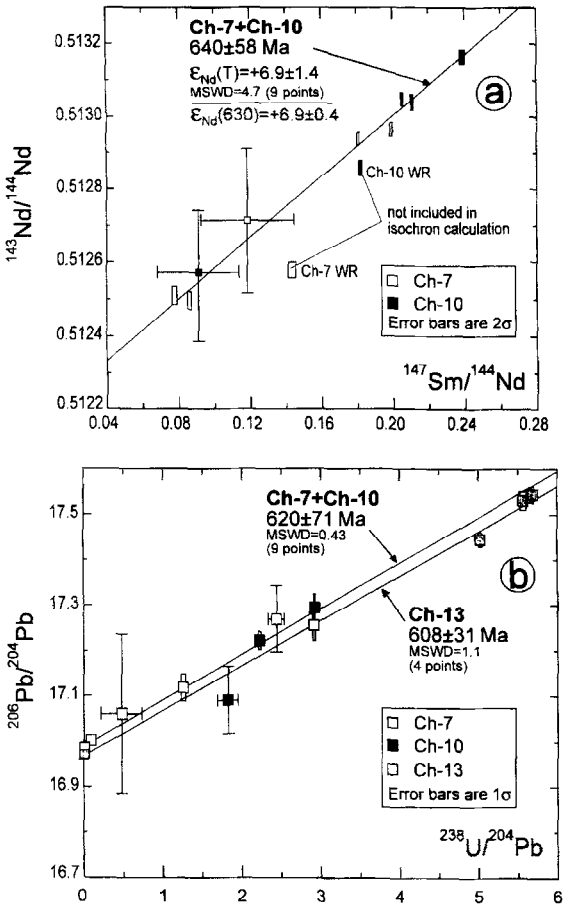

Fig. 6. (a) Sm–Nd mineral isochrons for harzburgites of the Chaya Massif. (b) U–Pb isochron diagram for minerals from ultramafic rocks of the Chaya Massif.

are shown in Fig. 6a. Mineral fractions from Ch-7 yield an errorchron (MSWD = 9.4) age of 625 ± 140 Ma. The pyroxene and an imprecise olivine analysis from Ch-10 plot on the same line, and the regression of these nine analyses together yields the apparent harzburgite Sm–Nd age of 640 ± 58 Ma, similar to the age of the mafic units. The whole-rock analyses of both harzburgites plot below the mineral best-fit line, well outside error limits.

4.3. U–Pb systematics

The U–Pb data for the minerals from harzburgites Ch-7 and Ch-10 (Table 3) plot on a single line in the $^{238}U/^{204}Pb$–$^{206}Pb/^{204}Pb$ evolution diagram (Fig. 6b). The slope of this line corresponds to the age of 620 ± 71 Ma, identical to the Sm–Nd age of the same fractions of 640 ± 58 Ma, and with the age of the Chaya mafic units. The $^{238}U/^{204}Pb$–$^{206}Pb/^{204}Pb$ mineral isochron for the websterite Ch-13 yields 619 ± 42 Ma (Fig. 6b), consistent with the other age determinations for the Chaya Massif.

The initial $^{207}Pb/^{204}Pb$ and $^{206}Pb/^{204}Pb$ ratios in samples Ch-7, Ch-10 and Ch-13 are calculated as weighted averages of in situ U-decay corrected Pb isotopic ratios for individual mineral fractions (Table 3, Fig. 7). The low $^{238}U/^{204}Pb$ ratios of 0.003–0.09 in three plagioclase fractions from samples Ch-7 and Ch-13 indicate that the correction for in situ U decay

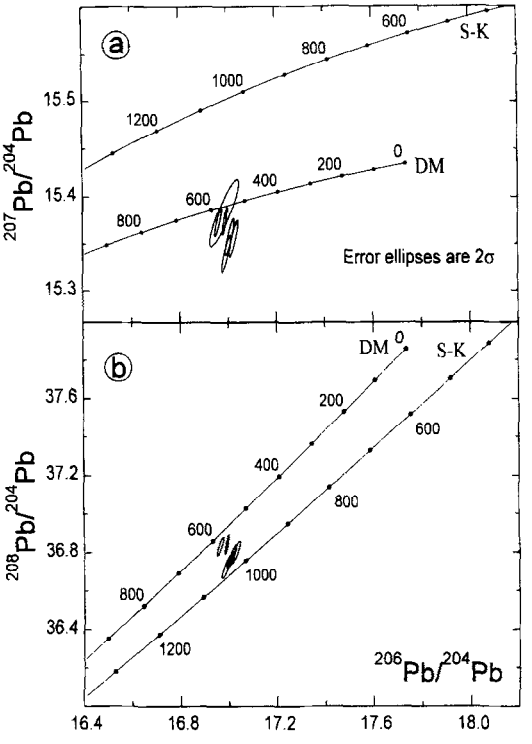

Fig. 7. Pb isotope data for the Chaya Massif. Each error ellipse represents an initial Pb isotopic composition of one sample. Initial $^{207}Pb/^{204}Pb$ and $^{206}Pb/^{204}Pb$ ratios in samples Ch-7, Ch-10 and Ch-13 are calculated as weighted averages of in situ U-decay corrected Pb isotopic ratios for individual mineral fractions. Plagioclase and data for other samples and all $^{208}Pb/^{204}Pb$ ratios are plotted without U-decay correction and are thought to approximate initial ratios (see text for details). Evolution curves for the average crust ($S-K$) and the depleted mantle (DM) are after Stacey and Kramers [52] and Neymark [19].

Table 3
U–Pb data

Sample	Fraction	Fraction weight (mg)	Lab.	U (ppm)	Pb (ppm)	$^{238}U/^{204}Pb$	$^{206}Pb/^{204}Pb$	$^{207}Pb/^{204}Pb$	$^{208}Pb/^{204}Pb$	$^{206}Pb/^{204}Pb$ (627 Ma)	$^{207}Pb/^{204}Pb$ (627 Ma)
Ch-4	Pl	> 200	IPGG				16.993 ± 16	15.340 ± 16	36.733 ± 50		
Ch-7	Pl-1	2.99	ROM	0.0020	1.321	0.0922 ± 44	17.004 ± 18	15.385 ± 20	36.872 ± 64	16.995 ± 18	15.385 ± 20
Ch-7	Pl-2	2.59	ROM	0.0004	1.686	0.0156 ± 36	16.987 ± 16	15.368 ± 18	36.823 ± 56	16.985 ± 16	15.368 ± 18
Ch-7	Cpx	3.07	ROM	0.0437	2.116	1.256 ± 53	17.118 ± 60	15.374 ± 54	36.906 ± 144	16.990 ± 72	15.366 ± 54
Ch-7	Opx-1	4.70	ROM	0.0036	0.092	2.439 ± 200	17.268 ± 144	15.504 ± 124	37.288 ± 316	17.019 ± 166	15.489 ± 124
Ch-7	Opx-2	7.72	ROM	0.0046	0.096	2.915 ± 31	17.255 ± 68	15.380 ± 58	37.048 ± 188	16.957 ± 112	15.362 ± 58
Ch-7	Ol	0.98	ROM	0.0002	0.031	0.48 ± 52	17.060 ± 350	15.419 ± 288	36.838 ± 544	17.011 ± 364	15.416 ± 288
Ch-10	Cpx	7.92	ROM	0.0525	1.444	2.221 ± 33	17.222 ± 40	15.395 ± 38	37.060 ± 104	16.995 ± 80	15.381 ± 38
Ch-10	Opx	14.84	ROM	0.0059	0.125	2.920 ± 19	17.294 ± 60	15.412 ± 52	37.197 ± 142	16.996 ± 108	15.394 ± 52
Ch-10	Ol	6.17	ROM	0.0004	0.012	1.82 ± 25	17.090 ± 148	15.350 ± 128	36.810 ± 316	16.904 ± 176	15.341 ± 128
Ch-13	Pl	> 200	IPGG				16.956 ± 16	15.373 ± 16	36.813 ± 50		
Ch-13	Pl	5.78	ROM	0.0002	3.712	0.0026 ± 26	16.970 ± 20	15.373 ± 22	36.867 ± 64	16.970 ± 20	15.375 ± 22
Ch-13	Cpx	6.50	ROM	0.0177	0.192	5.694 ± 25	17.544 ± 36	15.403 ± 34	37.534 ± 90	16.962 ± 180	15.368 ± 36
Ch-13	Opx-1	9.00	ROM	0.0027	0.030	5.568 ± 88	17.530 ± 40	15.361 ± 36	37.304 ± 104	16.961 ± 180	15.326 ± 40
Ch-13	Opx-2	10.9	ROM	0.0026	0.032	5.030 ± 53	17.445 ± 34	15.360 ± 30	37.272 ± 92	17.931 ± 162	15.329 ± 34
Ch-14	Pl	> 200	IPGG				17.009 ± 16	15.358 ± 16	36.780 ± 50		
Ch-15	Pl	> 200	IPGG				17.025 ± 16	15.356 ± 16	36.800 ± 50		
Ch-16	Pl	> 200	IPGG				16.976 ± 16	15.338 ± 16	36.707 ± 50		

Errors in U/Pb and Pb isotopic ratios are 2σ (see text for details).
Pl-1 in Ch-7 is a fraction of pale brown to reddish cloudy fragments; Pl-2 is a fraction of colorless, clear to slightly cloudy fragments.
Opx-1 in Ch-7 and Ch-13 are fractions of the best grains; Opx-2 is a bulk Opx fraction.
Errors in initial ratios (2σ) are propagated to include uncertainties in U/Pb and Pb isotopic ratios and age.

is negligible. The measured isotopic ratios for plagioclase from mafic samples, for which U and Pb concentrations were not determined, are thus thought to be representative of initial Pb isotopic ratios. The initial Pb ratios for the ultramafic samples and the measured plagioclase data for the mafic samples plot as a single compact cluster with mean $^{206}Pb/^{204}Pb = 16.994 \pm 0.023$ ($2\sigma_m$) and $^{207}Pb/^{204}Pb = 15.363 \pm 0.015$ ($2\sigma_m$) close to the depleted mantle evolution curve [19]. The single-stage model μ_1 values for sources of the Chaya Massif rocks, derived from intersections of 627–0 Ma secondary $^{207}Pb/^{204}Pb$–$^{206}Pb/^{204}Pb$ isochrons with the primary 4550–627 Ma isochron, range between 8.02 and 8.09, with the mean value of 8.07 ± 0.04 ($2\sigma_m$). The model $^{232}Th/^{238}U$ source values (κ_1), calculated assuming single-stage evolution from 4550 to 627 Ma, are between 3.95 and 4.02, with the mean value of 3.98 ± 0.02 ($2\sigma_m$).

4.4. Rb–Sr systematics

The initial Sr isotopic ratios in minerals and whole rocks of two harzburgites and one pyroxenite are presented in Table 2 and shown on Fig. 8 as $\varepsilon_{Sr}(627)$ values. All analyzed fractions of pyroxenite Ch-13 have nearly uniform $\varepsilon_{Sr}(627)$, between −7.7 and −9.5. The harzburgites Ch-7 and Ch-10 show more complex patterns. In Ch-7, clinopyroxene and olivine have the lowest Sr isotopic ratios, both measured and initial. The ratios in orthopyroxene and two plagioclase fractions are slightly higher. In Ch-10, the lowest $\varepsilon_{Sr}(627)$, of about −15.8, is determined in clinopyroxene and the fraction of the best hand picked orthopyroxene grains. The bulk orthopyroxene fraction has a higher $\varepsilon_{Sr}(627)$ value than the best orthopyroxene fraction, and substantially higher Rb, Sr, Sm and Nd concentrations (but similar U and Pb concentrations). The concentration of Sr in the olivine Ch-10 is too low to yield precise isotopic composition from the small sample analyzed. Whole-rock analyses of the harzburgites Ch-7 and Ch-10 show higher measured and initial Sr isotopic ratios and Rb/Sr than any analyzed mineral fractions from these rocks, clearly indicating the presence of secondary alteration-related mineral phases with elevated Rb and Rb/Sr.

The $\varepsilon_{Sr}(627)$ whole-rock values from the upper

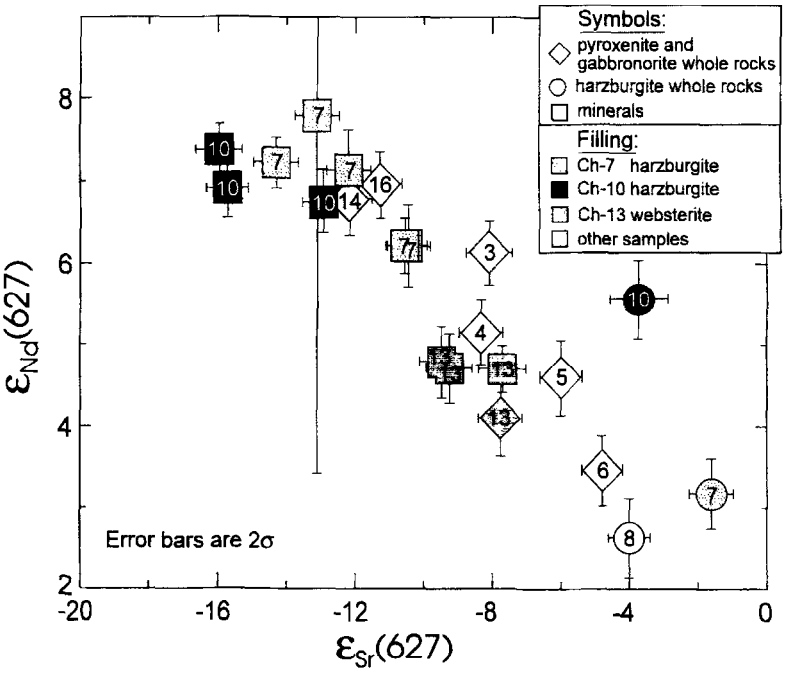

Fig. 8. Initial Nd and Sr isotopic values in whole rocks and mineral fractions from the Chaya Massif. Numbers within the symbols are abbreviated sample numbers (e.g. '3' corresponds to sample Ch-3).

and lower mafic units fall into two groups: −8.1 to −8.3 in the upper unit (samples Ch-3, Ch-4), and −11.3 to −12.2 in the lower unit (Ch-14, Ch-15 and Ch-16). The pyroxenite whole-rock $\varepsilon_{Sr}(627)$ vary between −4.8 and −7.8. None of the analyzed mafic rocks or pyroxenites have $\varepsilon_{Sr}(627)$ as low as in the harzburgite clinopyroxenes Ch-7 and Ch-10.

5. Discussion

5.1. Significance of alteration and implications for isotopic studies of ultramafic rocks

The effects of hydrothermal alteration in ophiolites on isotopic systems are well known [3,20–22]. Several lines of evidence suggest that the isotopic disequilibrium between minerals and whole rocks in the Chaya harzburgites Ch-7 and Ch-10 is caused by post-crystallization hydrothermal alteration: (1) higher measured and calculated initial $^{87}Sr/^{86}Sr$ ratios as well as Rb/Sr in whole rocks relative to values measured for primary minerals in the same rocks; and (2) higher concentrations of Rb, Sr, Sm and Nd and $\varepsilon_{Sr}(627)$ in the bulk orthopyroxene fraction of Ch-10, which may have contained some more altered grains, compared to the carefully hand picked orthopyroxene fraction from the same sample. The elevated whole-rock Rb/Sr ratios may indicate an addition of Rb during alteration, and the elevated $^{87}Sr/^{86}Sr$ suggests an external source of radiogenic Sr.

The isotopic pattern of alteration in the Chaya harzburgites (Fig. 8) is different from that commonly observed in mafic igneous rocks that have interacted with sea water. The most prominent difference is the large shift in $\varepsilon_{Nd}(627)$ between whole rocks and primary mafic minerals in the Chaya harzburgites: a difference of at least 2–4 ε units, and possibly larger, if the harzburgite Ch-8 had primary $\varepsilon_{Nd}(627)$ of about +7, similar to that in Ch-7 and Ch-10. At the same time, the shift in apparent initial Sr isotopic composition of about 12 ε units is small compared to the shifts of 40–90 ε units in ophiolites altered by interaction with sea water [21,23]. These features suggest that a fluid that interacted with the Chaya harzburgites had a relatively low Sr/Nd ratio. Models proposed to explain the displacement of initial Nd from primary magmatic values in sea water-altered ophiolites [21,22] involve complex, multi-stage equilibration of seawater-derived fluids with volcanic rocks, causing an increase in Nd concentrations. A similar process might have caused the mineral–whole rock isotopic disequilibria in the Chaya Massif. In addition, the hydrothermal alteration may be related to syn- or post-obduction processes, in which fluids could have interacted with the continental sediments or bedrocks. Sometimes ultramafic portions of ophiolites bear evidence for two episodes of hydrothermal alteration, early oceanic and late continental [24], both of which might have affected the isotopic systems.

Our data support the view that clinopyroxene is the best mineral for isotopic studies of ultramafic rocks. However, analysis of several primary minerals: clinopyroxene, orthopyroxene, olivine, and, if present, plagioclase, provides the potential for direct geochronological study of ultramafic rocks, which is not attainable with clinopyroxene alone. Consistency between Sm–Nd and U–Pb mineral isochron ages of the harzburgites Ch-7 and Ch-10 strongly suggests that these ages, and corresponding initial ratios, are geologically meaningful. Hand picking and acid leaching thus appeared to be efficient means for removing alteration products and recovering primary Sm–Nd and U–Pb isotopic data. The effect of alteration on the Rb–Sr system is reduced, but probably not completely eliminated, as indicated by internal variability of initial Sr ratios (cf. [25]). The petrogenetic implications of the Sr isotopic data are therefore considered tentative in the further discussion.

Low REE and Sr concentrations in ultramafic samples Ch-5, Ch-6 and Ch-8, similar to those in Ch-7 and Ch-10, suggest that the isotopic impact of alteration may be comparable to that observed for Ch-7 and Ch-10. Since we have not analyzed minerals from these samples, their whole-rock Nd and Sr initial ratios are considered suspect and are not used in the discussion of primary isotopic heterogeneity. An attempt to use whole-rock isotopic data for altered ultramafic rocks without analyzing primary minerals can result in misleading and unfounded interpretations. The case where the isotopic shifts due to alteration mimic a trend of variations in primary isotopic compositions, as observed in the Chaya Massif (Fig. 8), requires an especially careful

approach to data interpretation. We therefore recognize the need to revise our previous interpretation of relationships between ultramafic and mafic rocks in the Chaya Massif, which was based only on whole-rock Nd and Sr data [26].

5.2. Relationship between harzburgites and mafic cumulates

Dating of harzburgites and both lower and upper mafic cumulate units of the Chaya Massif using Sm–Nd and U–Pb mineral isochrons have shown that they are coeval at ca. 630 Ma. The coincidence of ages can allow either a genetic relationship between peridotites and mafic cumulates, or indicate complete resetting of the isotopic systems in harzburgite minerals during the formation of the mafic crustal sequences. On the basis of their initial Nd values, the studied rocks can be divided into two groups: (1) harzburgites and the lower mafic unit gabbronorites with $\varepsilon_{Nd} = +6.6$ to $+7.1$ and $\varepsilon_{Sr} = -11$ to -16; and (2) gabbronorites of the upper mafic unit and websterite of the lower unit: $\varepsilon_{Nd} = +4.6$ to $+6.1$ and $\varepsilon_{Sr} = -8$ to -9. Initial Pb isotopic ratios are identical in all these rocks, with the mean values $^{206}Pb/^{204}Pb = 16.994 \pm 0.023$ and $^{207}Pb/^{204}Pb = 15.363 \pm 0.015$. The small apparent initial Sr isotopic variability in the first group and the Sr isotopic distinction between the groups cannot be considered real until reliable initial Sr data are obtained for the minerals from both mafic and ultramafic rocks.

The geochronological and isotopic data thus indicate that the harzburgites and the lower mafic unit may be either cogenetic or strongly affected by the same process. At least two conceptual models can explain this relationship, either: (1) the harzburgites represent a residue after generation of a magma isotopically similar to the parental magma of the lower mafic unit, or (2) the isotopic systems in harzburgites were reset by interaction with basaltic magmas during formation of the mafic crustal sequence. Major element compositions and mineralogical features of the Chaya Massif: low SiO_2 and high FeO in harzburgites, high SiO_2 and MgO, and high orthopyroxene abundance in pyroxenites, are consistent with interaction between a pre-existing peridotite and a basaltic magma. This process results in a decrease in MgO/FeO and SiO_2 in the peridotite and complementary changes in a liquid composition [27,28]. The subsequent crystallization of this high-MgO, high-SiO_2 liquid would produce a orthopyroxene-enriched cumulate similar to the Chaya pyroxenites. The relative uniformity of harzburgite composition throughout the Chaya Massif ([12] and the data in this study) and the predominance of orthopyroxene over clinopyroxene throughout the pyroxenitic unit suggest that the peridotite–basaltic magma interaction was rather extensive. In this case, the Nd–Sr–Pb isotopic signature of the pre-existing peridotite should be completely, or almost completely, reset by the interaction with basaltic magma (e.g. [29]).

An interaction between basaltic magma and pre-existing peridotite was invoked by Gruau et al. [30] to explain the large range of variations in initial Nd isotopic ratios in the Trinity ophiolite, while we argue that a similar process in the Chaya Massif resulted in isotopic homogenization within the harzburgite unit and between harzburgites and mafic magmatites. These interpretations are, however, not contradictory because the isotopic effects of melt–peridotite interaction should depend on the melt/rock ratio and the degree of depletion of a peridotite before interaction with a magma. The mineralogical and major element features of the Chaya Massif suggest that the melt/peridotite ratios were rather high. At the same time, the lower heavy REE concentrations in the Chaya harzburgites indicate that they were initially more depleted than the Trinity lherzolites studied in [30]. In addition, an observation of Gruau et al. (op. cit.) that the peridotites tend to have the same $\varepsilon_{Nd}(T)$ as their neighboring or enclosing gabbros suggests that the complete isotopic homogenization also occurred in the Trinity ophiolite on a local scale. On the other hand, the Chaya harzburgite samples were collected within a few tens of meters from the mafic units, and the internal parts of the harzburgite body may not necessarily show complete isotopic resetting.

5.3. Isotopic heterogeneity and the origin of the Baikal–Muya ophiolite belt

The Nd isotopic characteristics of the Chaya peridotites and lower mafic unit lie close to the evolution trend of the depleted mantle (e.g. [31,32]). The ε_{Nd}

for the upper mafic unit and websterite Ch-13 are lower than the typical DM values, and the Sr initial ratios are close to the upper limit of the model DM values at 627 Ma (ε_{Sr} about -15 to -28). Initial Pb isotopic ratios are similar to the DM values [19] at 627 Ma.

A number of recent studies suggest that most ophiolites represent fragments of island arc or back-arc basin lithosphere [33–36]. A model of suprasubduction-zone origin was also proposed for the Baikal–Muya ophiolite belt [9]. Isotopic criteria may help to distinguish between mid-ocean ridge and suprasubduction-zone ophiolites, because the latter can be expected to have patterns of initial isotopic ratios similar to island arcs. The range of variations in εNd observed in the Chaya Massif and the presence of groups of rocks with distinct ε_{Nd} are typical for most ophiolites with a suggested suprasubduction-zone origin [4,30,36–38]. The Sr isotope evidence is less certain because ophiolite rocks are usually affected by seawater alteration and the primary isotopic data can rarely be recovered. The identification of primary Pb isotopic signatures in relatively old ophiolites is also difficult because of high U/Pb ratios and the disturbance of their U–Th–Pb systems by the alteration [39]. The Chaya initial Pb ratios are similar to MORB [40] extrapolated back to 627 m.y. ago, and are close to the most primitive values found in late Proterozoic and Paleozoic ophiolites [31,41]. The Pb isotopic data also do not rule out the suprasubduction-zone origin of the Baikal–Muya belt, since the most primitive island arc Pb isotopic compositions coincide with the MORB field (e.g. [42]).

The Nd, Sr and Pb isotopic data for the Chaya Massif thus plot on the overlap between the MORB and island arc fields and do not provide decisive evidence for the tectonic setting of the formation of the Baikal–Muya ophiolite belt. We leave this question open until detailed trace element data are available. The implications of ages determined in this study will be discussed elsewhere in a broader context of regional geology and geochronology.

6. Conclusions

Using a combination of hand picking and acid leaching allowed us to recover geochronological and the initial isotopic information from primary rock-forming and accessory minerals (olivine, orthopyroxene, clinopyroxene and plagioclase) from hydrothermally altered harzburgite. The Sm–Nd and U–Pb isochrons for minerals from the two harzburgite samples of the Chaya Massif yielded consistent ages of 640 ± 58 Ma and 620 ± 71 Ma, respectively, similar to the Sm–Nd age of the mafic units of 627 ± 25 Ma. The effect of alteration on the Rb–Sr system in the same mineral fractions is reduced, but probably not completely eliminated, as indicated by the internal variability of initial Sr ratios. The Rb–Sr and Sm–Nd systems in the whole-rock harzburgite samples are shown to be disturbed by hydrothermal alteration.

Similarity in ages and initial isotopic ratios between the harzburgites and the lower mafic unit in the Chaya Massif may indicate their close relationship. In accordance with the geological and chemical evidence for extensive interaction of pre-existing depleted peridotite with basaltic magma in the Chaya Massif, we suggest that the isotopic systems in the harzburgites were completely reset by the interaction with basaltic melt parental to the lower mafic unit. This interaction might have occurred during formation of a deep (intrusive) part of an island arc.

Acknowledgements

We wish to thank G.V. Ovchinnikova for help with Pb isotopic work at the IPGG, I.K. Shuleshko and group (IPGG) for separation of mineral concentrates, D.Z. Zhuravlev (IGEM) for REE analyses, and B. Podstawskji for mass spectrometer maintenance at the ROM. Comments of J. Morris and J. Paces and reviews by K. Johnson, P. Kelemen and M. Sharma helped to improve the manuscript. Financial support was provided by a Russian Foundation for Basic Research grant 95-05-15104C and by a NSERC operation grant to T.E. Krogh. *[FA]*

Appendix A

A.1. Analytical procedures

Mineral fractions were separated at the Institute of Precambrian Geology and Geochronology (IPGG)

using conventional magnetic and heavy liquid techniques. Mineral separates from mafic samples Ch-4, Ch-14 and Ch-16, analyzed for Sm–Nd at the IPGG, were cleaned in acetone and ultra pure water to remove the remaining traces of heavy liquids and handling contamination, and were not subjected to acid leaching. Plagioclase fractions for Pb isotopic analyses at the IPGG were washed in 1 N HNO_3, powdered in agate mortar and leached in hot, 12 N HNO_3 to remove possible radiogenic Pb components and U-bearing phases. Mineral fractions analyzed at the Royal Ontario Museum (ROM), represented by grain fragments, were hand picked in ethanol under a binocular microscope and examined at high magnification for absence of visible inclusions, fractures, turbidity and external grain surfaces. Both analyzed olivine fractions contained small fluid inclusions. The plagioclase and pyroxene fractions were subsequently washed in warm 6 N HCl and 7 N HNO_3, ultra pure water (thrice) and distilled acetone. This treatment was found to severely attack olivine, so the olivine fractions were washed in cold 2 N HCl.

Samples analyzed at the IPGG were spiked with ^{85}Rb–^{84}Sr and ^{149}Sm–^{146}Nd mixed tracers (100–150 mg mafic rocks and ca. 400 mg ultramafic rocks), or only ^{149}Sm–^{146}Nd tracer (mineral fractions, 100–150 mg) and dissolved in HF–HNO_3 in screw-capped PTFE vials. Insoluble chromite residue present in some samples was removed by centrifugation. Procedures of Rb–Sr, Sm–Nd and Pb isotopic analyses are similar to those described in [43].

Mineral fractions analyzed at the ROM were spiked with mixed ^{87}Rb–^{84}Sr, ^{149}Sm–^{150}Nd and ^{235}U–^{205}Pb tracers and dissolved in HF–HNO_3 in 3 ml Savillex PFA vials. Fraction weights are shown in Tables 2 and 3. Uranium and Pb were separated using an HCl–HBr–HNO_3 anion exchange procedure and loaded together on Re single filaments with SiO_2 emitter. An additional step of resin cleaning in 7 N HNO_3 reduced the U blank to 0.25 pg. Filtrates of the anion exchange columns were further processed for Rb, Sr, Sm and Nd separations, similar to those used at the IPGG, except for the smaller column sizes (1.8 cm^3 of cation exchange resin and

Table 4
Standard and blank data

Isotopic ratio [a]	Sample	IPGG (1988–89)	ROM (1992–93)	Δ = ROM − IPGG
$^{87}Sr/^{86}Sr$ [b]	SRM-987	0.710248 ± 0.000035	0.710241 ± 0.000027	−0.000007 (0.001%)
$^{87}Sr/^{86}Sr$ [b]	BCR-1	0.705010 ± 0.000030	0.705009 ± 0.000030	−0.000001
$^{87}Rb/^{86}Sr$	BCR-1	0.4080 ± 0.0020	0.4102 ± 0.0008	0.0022(0.54%)
$^{143}Nd/^{144}Nd$ [c] (Nd^+)	La Jolla	0.511848 ± 0.000020	0.511858 ± 0.000014	0.000010 (0.20 ε units)
$^{143}Nd/^{144}Nd$ (NdO^+)	La Jolla	–	0.511864 ± 0.000012	0.000016 (0.31 ε units)
$^{143}Nd/^{144}Nd$ [b]	BCR-1	0.512621 ± 0.000018	0.512638 ± 0.000008	0.000017 (0.33 ε units)
$^{143}Nd/^{144}Nd$ (NdO^+)	BCR-1	–	0.512648 ± 0.000014	0.000027 (0.53 ε units)
$^{143}Nd/^{144}Nd$	BCR-1	0.512633	0.512640 (Nd^+)	0.000007 (0.14 ε units)
(adjusted to 0.51186 in LJ)			0.512644 (NdO^+)	0.000011 (0.21 ε units)
$^{147}Sm/^{144}Nd$	BCR-1	0.13830 ± 30	0.13843 ± 15	0.00013 (0.094%)
$^{206}Pb/^{204}Pb$	BCR-1		18.796 ± 22	
$^{207}Pb/^{204}Pb$	BCR-1		15.609 ± 24	
$^{208}Pb/^{204}Pb$	BCR-1		38.656 ± 86	
Average blanks (pg) [a]	Rb	50	2.5 ± 1.5	
	Sr	600	35 ± 15	Pb blank IC at the ROM [a]:
	Sm	70	15 ± 8	$^{207}Pb/^{206}Pb = 0.853 \pm 5$
	Nd	300	28 ± 15	$^{208}Pb/^{206}Pb = 2.061 \pm 14$
	U	–	0.25 ± 0.15	$^{206}Pb/^{204}Pb = 17.9 \pm 6$
	Pb	5,000	5 ± 2	

[a] Quoted errors are 2 standard deviations.

[b] Unspiked and spiked runs in both laboratories, including spike calibration measurements with mixed standard Rb–Sr solutions made of SRM-987 Sr carbonate.

[c] Fractionation corrections of La Jolla runs in both laboratories were done using both standard exponential normalization and on-line isotope dilution program. No systematic differences were noticed.

0.25 cm^3 of HDEHP-coated Teflon powder). Rubidium was loaded on single Re filaments with SiO_2 gel; Sr was loaded on Ta single filaments with H_3PO_4. Both Sm and Nd were loaded with SiO_2 gel on single Re filaments and analyzed as MO^+ ions [44]. Lead fractions larger than 1 ng, Sm and Rb were measured in static multicollector mode on a 6-collector VG-354 mass spectrometer, calibrated for collector efficiencies using stable ion beam. Lead fractions smaller than 1 ng and U were analyzed using a Daly photomultiplier. Isotopic ratios of Nd and Sr, measured in dynamic multicollector mode, were normalized to $^{146}Nd/^{144}Nd = 0.7219$ and $^{88}Sr/^{86}Sr = 8.37521$ using exponential fractionation law. Nd analyses used all 6 collectors and included measurement of all Nd oxide peaks and monitoring of $^{140}Ce^{16}O$, $^{141}Pr^{16}O$ and $^{147}Sm^{16}O$ (corrected for Nd oxide) for possible interferences. A CeO^+ beam decayed rapidly at the optimum temperature for Nd ionization. A $^{141}Pr^{16}O$ signal was always present during analyses, being about 0.1–0.5 of the intensity of $^{144}Nd^{16}O$, so $^{143}Nd^{16}O$ was corrected for $^{141}Pr^{18}O$ interference. The ^{147}Sm was always below 10^{-5} of ^{144}Nd. Oxygen isotopic ratios $^{18}O/^{16}O = 0.00214 \pm 2$ ($2\sigma_m$) and $^{17}O/^{16}O = 0.000397 \pm 2$, measured using the $^{150}NdO^+$ ion beam of ^{150}Nd spike loads, were applied for oxygen isotope correction of Nd and Sm measurements. These values are higher than those reported by Wasserburg et al. [45] and Thirlwall [44] and are similar to the values obtained by Nyquist [45]. The large uncertainties of oxygen isotope composition are due to fractionation during analyses, with the entire range of 1.5% amu^{-1}.

The data reported in this paper were obtained in two laboratories using different procedures, so the inter-laboratory calibration is important for consistency of the data set. Standard results for Sm–Nd and Rb–Sr from both laboratories are presented in Table 4. The measured $^{87}Sr/^{86}Sr$ are in excellent agreement, while the $^{143}Nd/^{144}Nd$ ratios show differences of about 0.3–0.5 ε units (within the 2 s.d. error limits). Correction for accepted the $^{143}Nd/^{144}Nd$ value in La Jolla standard reduced the apparent inter-laboratory difference in $^{143}Nd/^{144}Nd$ for BCR-1 to 0.14–0.21 ε units, well within the reproducibility limits. The inter-laboratory difference in $^{147}Sm/^{144}Nd$ was about 0.1%, and the resulting bias in initial Nd ratios is negligible (0.01–0.02 ε units). The difference of 0.5% in $^{87}Rb/^{86}Sr$, measured in BCR-1, results in a shift of initial $^{87}Sr/^{86}Sr$ of 0.003% (within reproducibility limits) for a sample with the highest $^{87}Sr/^{86}Sr$ of 0.26, and is insignificant for the other samples. We therefore conclude that the inter-laboratory biases are well within the reproducibility limits and cannot be the reason for significant differences in isotopic systematics between minerals and whole rocks observed in this study.

Another possible source of uncertainty is the blank contribution. All concentrations and element ratios presented in Tables 2–4 are corrected for average blanks (Table 4) with appropriate error propagation. The Rb and Sr blanks were insignificant for all analyses, except the two olivine fractions. The Sm and Nd blank correction was significant for small orthopyroxene and plagioclase fractions analyzed at the ROM, and, to a lesser extent, for ultramafic whole-rock samples and some orthopyroxene and plagioclase fractions with low REE concentrations analyzed at the IPGG. A very large blank correction, 20–60%, was applied to Sm and Nd in olivine fractions, and their corrected $^{147}Sm/^{144}Nd$ ratios are therefore rather imprecise. The U blanks are significant for olivine, orthopyroxene and small plagioclase fractions but their effect on absolute errors of U/Pb ratios in plagioclase is very small because of low U/Pb. The Pb blank correction is small for all fractions except olivine and orthopyroxene. However, correction for U and Pb blanks was applied to all fractions studied at the ROM as a part of a data reduction routine [46].

The REE concentrations were measured in separate powder aliquots at the Institute for the Geology of Ore Deposits, Petrography, Mineralogy and Geochemistry of the Russian Academy of Science, Moscow (IGEM), using the isotope dilution technique [47]. The accuracy and precision of REE determinations are $\pm 3\%$ for La and better than $\pm 2\%$ for the other REE.

Isochron calculations were performed using the ISOPLOT program [48]; the ages are presented at the 95% confidence level. The Nd and Sr isotopic compositions are given in ε notation using CHUR parameters of Jacobsen and Wasserburg [49] and $(^{87}Sr/^{86}Sr)0 = 0.7045$, $^{87}Rb/^{86}Sr = 0.0827$ for the mantle uniform reservoir (UR).

References

[1] M. Sharma, D.A. Papanastassiou, G.J. Wasserburg, M. Roy Barman, Relative chronology of tectonites and layered sequences in ophiolite complexes, Geol. Soc. Am. Abstr. with Progr. 26 (7) (1994) A29.

[2] C. Göpel, C.J. Allègre, Xu Rong-Hua, Lead isotopic study of the Xigaze ophiolite (Tibet): the problem of the relationship between magmatites (gabbros, dolerites, lavas) and tectonites (harzburgites), Earth Planet. Sci. Lett. 69 (1984) 301–310.

[3] M. Sharma, G.J. Wasserburg, D.A. Papanastassiou, J.F. Quick, E.V. Sharkov, E.E. Laz'ko, High $^{143}Nd/^{144}Nd$ in extremely depleted mantle rocks, Earth Planet. Sci. Lett. 135 (1995) 101–114.

[4] S.B. Jacobsen, J.E. Quick, G.J. Wasserburg, A Nd and Sr isotopic study of the Trinity peridotite: implications for mantle evolution, Earth Planet. Sci. Lett. 68 (1984) 361–378.

[5] K.A. Klitin, T.G. Pavlova, Ophiolite complex of the Baikal fold zone, Dokl. Acad. Sci. USSR Earth Sci. Sect. 215 (1-6) (1975) 33–36.

[6] N.L. Dobretsov, N.A. Berzin, M.M. Buslov, Opening and tectonic evolution of the Paleo-Asian Ocean, Int. Geol. Rev. 37 (1995) 335–360.

[7] E.G. Konnikov, On the problem of ophiolites of the Baikal–Muya belt, Sov. Geol. Geophys. 32 (3) (1991) 104–113.

[8] N.L. Dobretsov, E.G. Konnikov, N.N. Dobretsov, Precambrian ophiolite belts of southern Siberia, Russia, and their metallogeny, Precambrian Res. 58 (1992) 427–446.

[9] G.S. Gusev, A.I. Peskov, S.K. Sokolov, Paleodynamics of the Muy Segment, Proterozoic Baikal–Vitim belt, Geotectonics 26 (2) (1992) 142–152.

[10] M.I. Grudinin and I.A. Demin, Riphean ophiolites of the Northern Baikal Region (East Siberia), in: Proc. 29th Int. Geol. Congr., Part D, 1994, pp. 263–272.

[11] E.G. Konnikov, A.A. Tsygankov, T.I. Kazantseva, Geochemistry and correlation of the Precambrian ophiolites in the western margin of the Muya crystalline block, Geochem. Int. 31 (10) (1994) 76–86.

[12] F.P. Lesnov, Geology and petrology of the Chaya gabbro–peridotite–dunite nickel-bearing pluton, Nauka, Novosibirsk 1972. 228 pp. (in Russian).

[13] N.L. Dobretsov, Ophiolites and the problems of the Baikal–Muya ophiolite belt, in: Magmatism and Metamorphism of Baikal–Amur Railway Region, Nauka, Novosibirsk, 1983, pp. 11–19 (in Russian).

[14] G.A. McKay, Partitioning of rare earth elements between major silicate minerals and basaltic melts, in: B.R. Lipin, G.A. McKay (Eds.), Geochemistry and Mineralogy of Rare Earth Elements, Reviews in Mineralogy, Vol. 21, 1989, pp. 45–77.

[15] W.F. McDonough, F.A. Frey, Rare earth elements in upper mantle rocks, in: B.R. Lipin, G.A. McKay (Eds.), Geochemistry and Mineralogy of Rare Earth Elements, Reviews in Mineralogy, Vol. 21, 1989, pp. 99–145.

[16] C.J. Suen, F.A. Frey, J. Malpas, Bay of Islands ophiolite suite, Newfoundland: petrologic and geochemical characteristics with emphasis on rare earth element geochemistry, Earth Planet. Sci. Lett. 45 (1979) 337–348.

[17] A. Prinzhofer, C.J. Allègre, Residual peridotites and the mechanisms of partial melting, Earth Planet. Sci. Lett. 74 (1985) 251–265.

[18] M. Sharma, G.J. Wasserburg, The neodymium isotopic compositions and rare earth patterns in highly depleted ultramafic rocks, Geochim. Cosmochim. Acta 60 (1996) 4537–4550.

[19] L.A. Neymark, Lead isotopes, $^{Pb}T_{DM}$ parameter and the crustal pre-history of rocks, in: W. Compston (Ed.), 7th Int. Conf. on Geochronology, Cosmochronology and Isotope Geology,, Abstr. Geol. Soc. Aust. 27 (1990) 70.

[20] M.T. McCulloch, R.T. Gregory, G.J. Wasserburg, H.P. Taylor Jr., Sm–Nd, Rb–Sr, and $^{18}O/^{16}O$ isotopic systematics in an oceanic crustal section: evidence from the Semail ophiolite, J. Geophys. Res. 86 (1981) 2721–2735.

[21] R.L. Edwards, G.J. Wasserburg, The age and emplacement of obducted oceanic crust in the Urals from Sm–Nd and Rb–Sr systematics, Earth Planet. Sci. Lett. 72 (1985) 389–404.

[22] E. Valsami-Jones, J.R. Cann, Controls on the Sr and Nd isotopic compositions of hydrothermally altered rocks from the Pindos Ophiolite, Greece, Earth Planet. Sci. Lett. 125 (1994) 39–54.

[23] S.B. Jacobsen, G.J. Wasserburg, Nd and Sr isotopic study of the Bay of Islands ophiolite complex and the evolution of the source of mid-ocean ridge basalts, J. Geophys. Res. 84 (1979) 7429–7445.

[24] R. Laurent, Y. Hébert, Paragenesis of serpentine assemblages in harzburgite tectonite and dunite cumulate from the Québec Appalachians, Can. Mineral. 17 (1979) 857–869.

[25] J.E. Snow, S.R. Hart, H.J.B. Dick, Nd and Sr isotope evidence linking mid-ocean ridge basalts and abyssal peridotites, Nature 371 (1994) 57–60.

[26] Yu.V. Amelin, E.Yu. Ritsk, L.A. Neymark, G.V. Ovchinnikova, Nd–Sr–Pb isotopic variations in Chaya basic–ultrabasic massif (North Baikal region): implications for source heterogeneity and processes in magma chambers, in: Abstr. 29th Int. Geol. Congr. Kyoto, Vol. 2, 1992, p. 183.

[27] P.B. Kelemen, M.S. Ghiorso, Assimilation of peridotite in zoned calc-alkaline plutonic complexes: evidence from Big Jim complex, Washington Cascades, Contrib. Mineral. Petrol. 94 (1986) 12–28.

[28] P.B. Kelemen, Reaction between ultramafic rock and fractionating basaltic magma. I. Phase relationships, the origin of calc-alkaline magma series, and the formation of discordant dunite, J. Petrol. 31 (1990) 51–98.

[29] O. Navon, E. Stolper, Geochemical consequences of melt percolation: The upper mantle as a chromatographic column, J. Geol. 95 (1987) 285–307.

[30] G. Gruau, J. Bernard-Griffiths, C. Lecuyer, O. Henin Jr., J. Macé, M. Cannat, Extreme Nd isotopic variation in the Trinity Ophiolite Complex and the role of melt/rock reactions in the oceanic lithosphere, Contrib. Mineral. Petrol. 121 (1995) 337–350.

[31] H.F. Shaw, J.H. Chen, J.B. Saleeby, G.J. Wasserburg, Nd–Sr–Pb systematics and age of the Kings River ophiolite,

California: implications for depleted mantle evolution, Contrib. Mineral. Petrol. 96 (1987) 281–290.
[32] M. Zimmer, A. Kröner, K.P. Jochum, T. Reischmann, W. Todt, The Gabal Gerf complex: a Precambrian N-MORB ophiolite in the Nubian Shield, NE Africa, Chem. Geol. 123 (1995) 29–51.
[33] G. Sierri, The petrochemistry of ophiolite gabbroic complexes: a key for the classification of ophiolites into low-Ti and high-Ti types, Earth Planet. Sci. Lett. 52 (1981) 203–212.
[34] J.A. Pearce, S.J. Lippard, S. Roberts, Characteristics and tectonic significance of supra-subduction zone ophiolites, in: B.P. Kokelaar and M.F. Howells (Eds.), Marginal Basin Geology, Blackwell, 1984, pp. 77–94.
[35] R.B. Pedersen, J. Hertogen, Magmatic evolution of the Kamrøy ophiolite complex, SW Norway: relationships between MORB–IAT–boninitic–calc-alkaline and alkaline magmatism, Contrib. Mineral. Petrol. 104 (1990) 277–293.
[36] G.A. Jenner, G.R. Dunning, J. Malpas, M. Brown, T. Brace, Bay of Islands and Little Port complexes, revisited: age, geochemical and isotopic evidence confirm suprasubduction-zone origin, Can. J. Earth Sci. 28 (1991) 1635–1652.
[37] M.T. McCulloch, W.E. Cameron, Nd–Sr isotopic study of primitive lavas from the Troodos ophiolite, Cyprus: evidence for a subduction-related setting, Geology 11 (1983) 727–731.
[38] M. Rautenschlein, G.A. Jenner, J. Hertogen, A.W. Hofmann, R. Kerrich, H.-U. Schmincke, W.M. White, Isotopic and trace element composition of volcanic glasses from the Akaki canyon, Cyprus: implications for the origin of the Troodos ophiolite, Earth Planet. Sci. Lett. 75 (1985) 369–383.
[39] B. Hamelin, B. Dupré, O. Brévart, C.J. Allègre, Metallogenesis at paleo-spreading centers: lead isotopes in sulfides, rocks and sediments from the Troodos ophiolite (Cyprus), Chem. Geol. 68 (1988) 229–238.
[40] W.M. White, $^{238}U/^{204}Pb$ in MORB and open system evolution of the depleted mantle, Earth Planet. Sci. Lett. 115 (1993) 211–226.
[41] J.S. Pallister, J.S. Stacey, L.B. Fischer, W.R. Premo, Precambrian ophiolites of Arabia: geologic settings, U–Pb geochronology, Pb-isotope characteristics, and implications for continental accretion, Precambrian Res. 38 (1988) 1–54.
[42] C.J. Hawkesworth, J.M. Hergt, F. McDermott, R.M. Ellam, Destructive margin magmatism and the contributions from the mantle wedge and subducted crust, Aust. J. Earth Sci. 38 (1991) 577–594.
[43] Yu.V. Amelin, L.A. Neymark, E.Yu. Ritsk, A.A. Nemchin, Enriched Nd–Sr–Pb isotopic signatures in the Dovyren layered intrusion, Eastern Siberia: evidence for source contamination by ancient upper-crustal material, Chem. Geol. 129 (1996) 39–69.
[44] M.F. Thirlwall, High-precision multicollector isotopic analysis of low levels of Nd as oxide, Chem. Geol. (Isot. Geosci. Sect.) 94 (1991) 13–22.
[45] G.J. Wasserburg, S.B. Jacobsen, D.J. DePaolo, M.T. McCulloch, T. Wen, Precise determination of Sm/Nd ratios, Sm and Nd isotopic abundances in standard solutions, Geochim. Cosmochim. Acta 45 (1981) 2311–2323.
[46] Yu.V. Amelin, L.M. Heaman, V.M. Verchogliad, V.M. Skobelev, Geochronological constraints on the emplacement history of an anorthosite–rapakivi granite suite: U–Pb zircon and baddeleyite study of the Korosten complex, Ukraine, Contrib. Mineral. Petrol. 116 (1994) 411–419.
[47] I.S. Puchtel, D.Z. Zhuravlev, A.V. Samsonov, N.T. Arndt, Petrology and geochemistry of metamorphosed komatiites and basalts from the Tungurcha greenstone belt, Aldan Shield, Precambrian Res. 62 (1993) 399–417.
[48] K.R. Ludwig, ISOPLOT—a plotting and regression program for radiogenic isotope data, for IBM-PC compatible computers, version 2.57, USGS Open-File Rep. 91-445, 1992, 40 pp.
[49] S.B. Jacobsen, G.J. Wasserburg, Sm–Nd evolution of chondrites, Earth Planet. Sci. Lett. 50 (1980) 139–155.
[50] R.G. Coleman, Ophiolites—Ancient Oceanic Lithosphere?, Minerals and Rocks, Springer, Berlin, 1977, 229 pp.
[51] S.R. Taylor, S.M. McLennan, The Continental Crust, its Composition and Evolution, Blackwell, Oxford, 1985, 312 pp.
[52] J.S. Stacey, J.D. Kramers, Approximation of terrestrial lead evolution by a two-stage model, Earth Planet. Sci. Lett. 26 (1975) 207–221.